

Magnetic Circuit Model of PM Motor-Generator to Predict Radial Forces

Peter E. Kascak
University of Toledo, Toledo, Ohio

Timothy P. Dever
QSS Group, Inc., Cleveland, Ohio

Ralph H. Jansen
University of Toledo, Toledo, Ohio

The NASA STI Program Office . . . in Profile

Since its founding, NASA has been dedicated to the advancement of aeronautics and space science. The NASA Scientific and Technical Information (STI) Program Office plays a key part in helping NASA maintain this important role.

The NASA STI Program Office is operated by Langley Research Center, the Lead Center for NASA's scientific and technical information. The NASA STI Program Office provides access to the NASA STI Database, the largest collection of aeronautical and space science STI in the world. The Program Office is also NASA's institutional mechanism for disseminating the results of its research and development activities. These results are published by NASA in the NASA STI Report Series, which includes the following report types:

- **TECHNICAL PUBLICATION.** Reports of completed research or a major significant phase of research that present the results of NASA programs and include extensive data or theoretical analysis. Includes compilations of significant scientific and technical data and information deemed to be of continuing reference value. NASA's counterpart of peer-reviewed formal professional papers but has less stringent limitations on manuscript length and extent of graphic presentations.
- **TECHNICAL MEMORANDUM.** Scientific and technical findings that are preliminary or of specialized interest, e.g., quick release reports, working papers, and bibliographies that contain minimal annotation. Does not contain extensive analysis.
- **CONTRACTOR REPORT.** Scientific and technical findings by NASA-sponsored contractors and grantees.

- **CONFERENCE PUBLICATION.** Collected papers from scientific and technical conferences, symposia, seminars, or other meetings sponsored or cosponsored by NASA.
- **SPECIAL PUBLICATION.** Scientific, technical, or historical information from NASA programs, projects, and missions, often concerned with subjects having substantial public interest.
- **TECHNICAL TRANSLATION.** English-language translations of foreign scientific and technical material pertinent to NASA's mission.

Specialized services that complement the STI Program Office's diverse offerings include creating custom thesauri, building customized databases, organizing and publishing research results . . . even providing videos.

For more information about the NASA STI Program Office, see the following:

- Access the NASA STI Program Home Page at **<http://www.sti.nasa.gov>**
- E-mail your question via the Internet to **help@sti.nasa.gov**
- Fax your question to the NASA Access Help Desk at 301-621-0134
- Telephone the NASA Access Help Desk at 301-621-0390
- Write to:
NASA Access Help Desk
NASA Center for Aerospace Information
7121 Standard Drive
Hanover, MD 21076



Magnetic Circuit Model of PM Motor-Generator to Predict Radial Forces

Peter E. Kascak
University of Toledo, Toledo, Ohio

Timothy P. Dever
QSS Group, Inc., Cleveland, Ohio

Ralph H. Jansen
University of Toledo, Toledo, Ohio

Prepared for the
First International Energy Conversion Engineering Conference
sponsored by the American Institute of Aeronautics and Astronautics
Portsmouth, Virginia, August 17–21, 2003

Prepared under Cooperative Agreement NCC3-924

National Aeronautics and
Space Administration

Glenn Research Center

Available from

NASA Center for Aerospace Information
7121 Standard Drive
Hanover, MD 21076

National Technical Information Service
5285 Port Royal Road
Springfield, VA 22100

Available electronically at <http://gltrs.grc.nasa.gov>

MAGNETIC CIRCUIT MODEL OF PM MOTOR-GENERATOR TO PREDICT RADIAL FORCES

Peter E. Kascak
University of Toledo
Toledo, Ohio

Timothy P. Dever
QSS Group, Inc.
Cleveland, Ohio

Ralph H. Jansen
University of Toledo
Toledo, Ohio

Abstract

A magnetic circuit model is developed for a PM motor for flywheel applications. A sample motor is designed and modeled. Motor configuration and selection of materials is discussed, and the choice of winding configuration is described. A magnetic circuit model is described, which includes the stator back iron, rotor yoke, permanent magnets, air gaps and the stator teeth. Iterative solution of this model yields flux linkages, back EMF, torque, power, and radial force at the rotor caused by eccentricity. Calculated radial forces are then used to determine motor negative stiffness.

Introduction

High speed flywheel systems are currently under development at NASA Glenn Research Center (GRC) in Cleveland, Ohio. Flywheels are being considered as an alternative to batteries and reaction wheels in space vehicles. Strengths of this technology include high energy density, long life, deep depth of discharge, and pulse power capability. Also, flywheels can be deployed in an array which provides both energy storage and attitude control. A system level flywheel testbed is operational at GRC. The system uses active magnetic bearings to provide a long life, low-loss suspension of the rotor. Permanent magnet (PM) motor-generators are used to store and retrieve energy from the rotor.

This paper discusses a magnetic circuit model which will be used as a design tool for subsequent flywheel motor-generator designs. A sample motor-generator is developed to validate the design code. For simplicity, the motor-generator unit will be referred to simply as a motor for the remainder of the paper.

Nomenclature

“back iron”	designates stator back iron
“yoke”	designates rotor back iron
$A_{tooth-tip}$	cross sectional area of stator tooth tip
$B_{tooth-tip}$	flux density of stator tooth tip
d_s	slot depth
D_{ri}	rotor inner diameter
D_{so}	stator outer diameter
\mathbf{F}	MMF vector (A/turns)
$g_{mechanical}$	mechanical air gap
h	harmonic number
\mathbf{i}, \mathbf{j}	unit vectors in x and y direction
K_{dh}	winding distribution factor
K_{ph}	pitch factor
\mathfrak{R}	reluctance (H^{-1})
v_{emf}	back emf
W	coil pitch
W_{magnet}	permanent magnet thickness
W_{yoke}	yoke width
q	number of coils per phase belt
z	arc length of coils in winding group
ϕ	flux vector (Wb)
τ	torque
τ_p	pole pitch
λ	flux linkage
ω_{mech}	mechanical speed (rad/sec)

Design Approach

A variety of methods are brought together to design the motor. The following is a quick summary of the design approach used:

1. Select motor configuration and materials
2. Optimize fractional pitch
3. Optimize winding distribution factor
4. Define motor magnetic circuit model
5. Solve model iteratively for flux (360°)
6. Calculate flux linkages, and back EMF
7. Calculate power and torque versus angle
8. Calculate radial force versus rotor displacement

Details describing implementation of each of the above steps are presented in the following sections.

Motor Configuration

The motor configuration chosen for the flywheel design is a PM, radial gap, outer stator, inner rotor configuration; the motor will be a three phase, four pole design with 24 slots. This configuration was selected based on previous experience with motors used in flywheel applications; size of the motor is also defined by the specific application. The layout for this motor is shown schematically in Figure 1.

All of the iron parts (the stator back iron, the stator teeth and the rotor yoke) are made of an iron cobalt alloy, which was selected for its ability to carry high flux

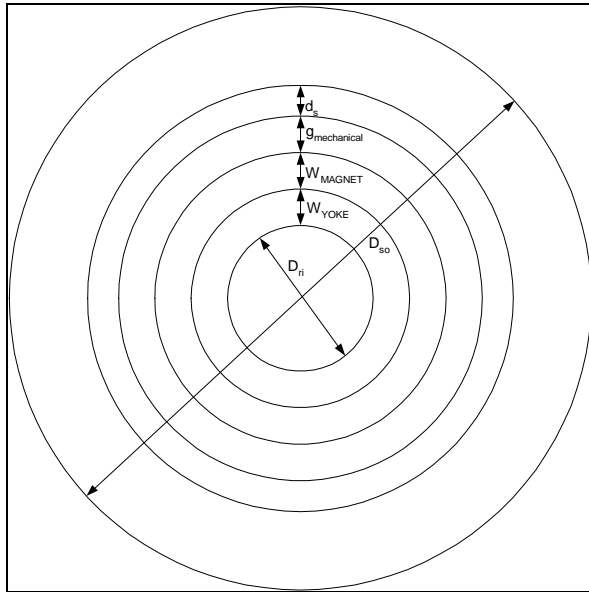


Figure 1. Motor configuration

densities (~2.2 Tesla), and for its high strength, which will allow high speed operation.

The two candidate permanent magnet materials were samarium cobalt and neodymium iron boron; samarium cobalt was selected due to its superior high temperature performance. For the analysis performed in this paper, the magnets are assumed to have constant radial magnetization.

Motor Winding Configuration

Next, the fractional pitch is selected, to optimize harmonic content of the MMF harmonics. The pitch factor for a given harmonic is given as [1]:

$$k_{ph} = \sin \left[\frac{hW}{\tau_p} \left(\frac{\pi}{2} \right) \right] \sin \left(\frac{h\pi}{2} \right) \quad (1)$$

The amplitude of the MMF harmonics is proportional to $\frac{k_{ph}}{h}$; we plot this versus the fractional pitch, which is

defined as $\frac{W}{\tau_p}$, and select fractional pitch to optimize

desired harmonic content. The plot is shown in Figure 2. Note that the harmonic number, h , has only odd values possible, since only odd harmonics exist in this motor.

For this design, we wish to minimize third harmonic content. One full pitch for this motor is 24 slots/4 poles = 6 slots; thus reasonable options are 3/6, 4/6, 5/6 fractional pitch or 6/6 full pitch. Since third harmonic

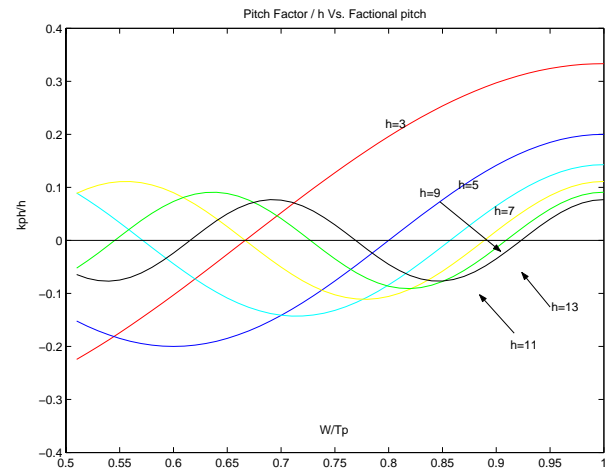


Figure 2. Pitch factor as a function of fractional pitch

content in Figure 2 is minimized with a pitch factor of 0.67, a coil pitch of 4 was selected.

The winding structure for the motor stator is double layer lap wound. The winding distribution factor is given as [1]:

$$k_{dh} = \frac{1}{q} \frac{\sin\left(\frac{hz}{\tau_p} \frac{\pi}{2}\right)}{\sin\left(\frac{hz}{\tau_p} \frac{\pi}{2q}\right)} \quad (2)$$

where z/τ_p is the fraction of a pole pitch that is occupied by the phase belt. With a four pole, three phase, 24 slot, 4/6 fractional pitch machine, each 360 electrical degree phase belt has four coils, and the only design options available are a 60° or a 120° phase belt. Since considerably more voltage is generated by a 60° phase belt (k_{d1} is 0.958 for a 60° phase belt versus 0.837 for a 120° phase belt), the 60° phase belt was selected.

With all three phases, 360 electrical degrees is spanned by 12 coils, at 30° increments. The electrical phase relationship of these coils is shown in Figure 3.

Figure 4 shows the MMF's of the coils when they are collected into 60° degree phase belts. Note that some of the coils are wound in with negative polarities.

Finally, the winding layout of all three phases is shown in Figure 5.

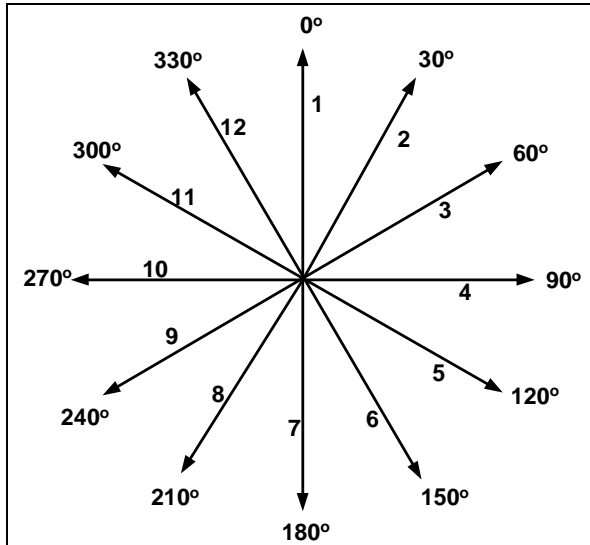


Figure 3. Coil electrical phase relationship

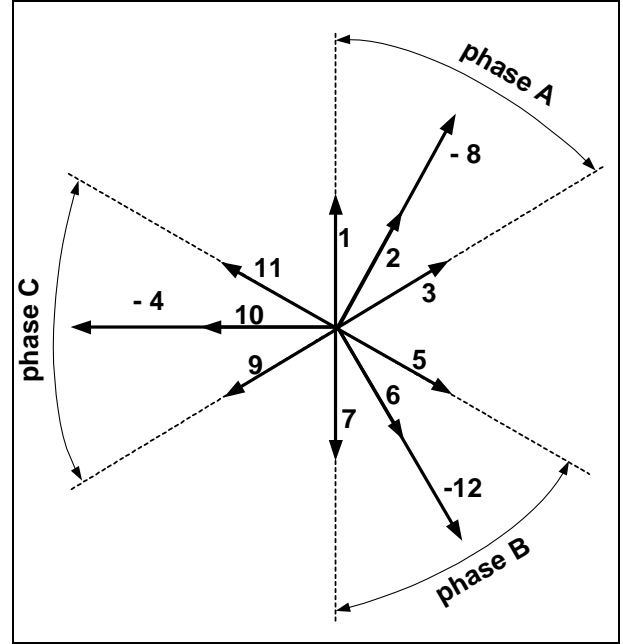


Figure 4. Coils with 60 degree phase belts

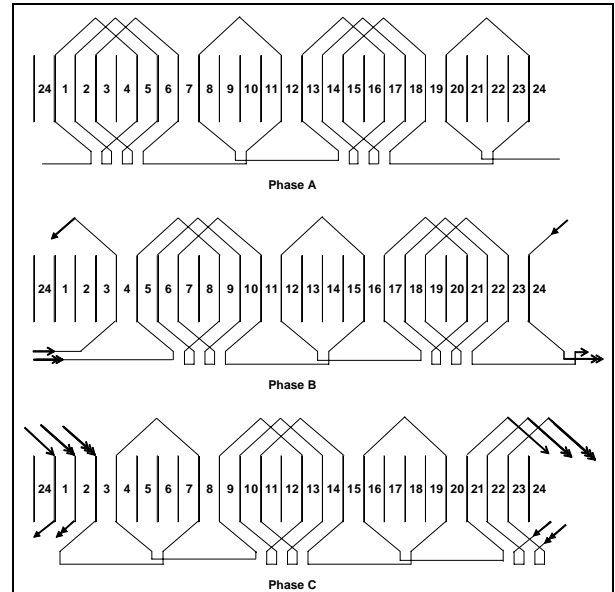


Figure 5. Winding layout for all three motor phases

Magnetic Circuit Model

Next, the motor is modeled as a magnetic circuit. Reluctance elements are included in the model for the back iron, stator teeth, air gap, and rotor yoke. MMF sources in the model include the PMs and the windings enclosing the stator teeth. The PM MMF is determined using the demagnetization curve for the magnetic material, and the windings that enclose each tooth are

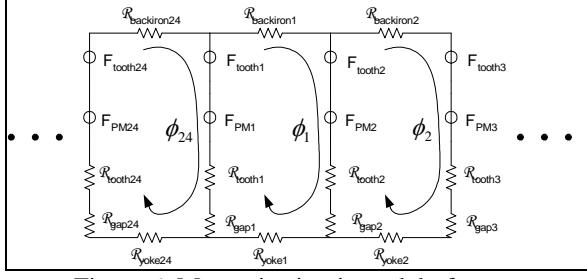


Figure 6. Magnetic circuit model of motor

summed together to determine the magnitude of the tooth MMF. The schematic of the motor magnetic circuit is shown in Figure 6.

This magnetic circuit is solved by mesh currents. Summing the MMF around the loop containing tooth 1 and tooth 2 yields:

$$\begin{aligned}
 & -\phi_1 \mathfrak{R}_{backiron1} - F_{tooth2} - F_{PM2} \\
 & -(\phi_1 - \phi_2)(\mathfrak{R}_{tooth2} + \mathfrak{R}_{gap2}) - \phi_1 \mathfrak{R}_{yoke1} \\
 & -(\phi_1 - \phi_{24})(\mathfrak{R}_{tooth1} + \mathfrak{R}_{gap1}) + \\
 & F_{PM1} + F_{tooth1} = 0
 \end{aligned} \quad (3)$$

Rearranging Eq. (3) yields:

$$\begin{aligned}
 & (-\mathfrak{R}_{backiron1} - \mathfrak{R}_{tooth2} - \mathfrak{R}_{gap2} \\
 & - \mathfrak{R}_{yoke1} - \mathfrak{R}_{tooth1} - \mathfrak{R}_{gap1})\phi_1 \\
 & + (\mathfrak{R}_{tooth2} + \mathfrak{R}_{gap2})\phi_2 + (\mathfrak{R}_{tooth1} + \mathfrak{R}_{gap1})\phi_{24} \\
 & = F_{tooth2} + F_{PM2} - F_{PM1} - F_{tooth1}
 \end{aligned} \quad (4)$$

Using Eq. (4), a generalized expression for loops 2 to 23 can be derived:

$$\begin{aligned}
 & (-\mathfrak{R}_{backiron(n)} - \mathfrak{R}_{tooth(n+1)} - \mathfrak{R}_{gap(n+1)} - \mathfrak{R}_{yoke(n)} \\
 & - \mathfrak{R}_{tooth(n)} - \mathfrak{R}_{gap(n)})\phi_n + \\
 & (\mathfrak{R}_{tooth(n+1)} + \mathfrak{R}_{gap(n+1)})\phi_{n+1} + \\
 & (\mathfrak{R}_{tooth(n)} + \mathfrak{R}_{gap(n)})\phi_{n-1} \\
 & = F_{tooth(n+1)} + F_{PM(n+1)} - F_{PM(n)} - F_{tooth(n)}
 \end{aligned} \quad (5)$$

Rewriting Eq. (5) for the case of loop 24 yields:

$$\begin{aligned}
 & (-\mathfrak{R}_{backiron24} - \mathfrak{R}_{tooth1} - \mathfrak{R}_{gap1} - \mathfrak{R}_{yoke24} \\
 & - \mathfrak{R}_{tooth24} - \mathfrak{R}_{gap24})\phi_{24} + (\mathfrak{R}_{tooth1} + \mathfrak{R}_{gap1})\phi_1 \\
 & (\mathfrak{R}_{tooth24} + \mathfrak{R}_{gap24})\phi_{23} \\
 & = F_{tooth1} + F_{PM1} - F_{PM24} - F_{tooth24}
 \end{aligned} \quad (6)$$

Using Eq. (5), define the following lumped reluctance quantities for the first 23 loops

$$\begin{aligned}
 X_n = & -\mathfrak{R}_{tooth(n)} - \mathfrak{R}_{gap(n)} - \mathfrak{R}_{backiron(n)} \\
 & - \mathfrak{R}_{tooth(n+1)} - \mathfrak{R}_{gap(n+1)} - \mathfrak{R}_{yoke(n)}
 \end{aligned} \quad (7)$$

$$Y_n = \mathfrak{R}_{tooth(n+1)} + \mathfrak{R}_{gap(n+1)} \quad (8)$$

$$Z_n = \mathfrak{R}_{tooth(n)} + \mathfrak{R}_{gap(n)} \quad (9)$$

Using Eq. (6), the lumped reluctance quantities for loop 24 are

$$\begin{aligned}
 X_{24} = & -\mathfrak{R}_{tooth24} - \mathfrak{R}_{gap24} - \mathfrak{R}_{backiron24} \\
 & - \mathfrak{R}_{tooth1} - \mathfrak{R}_{gap1} - \mathfrak{R}_{yoke24}
 \end{aligned} \quad (10)$$

$$Y_{24} = \mathfrak{R}_{tooth1} + \mathfrak{R}_{gap1} \quad (11)$$

$$Z_{24} = \mathfrak{R}_{tooth24} + \mathfrak{R}_{gap24} \quad (12)$$

Using Eq. (7) through (12), we now define the reluctance matrix as:

$$\mathfrak{R} \equiv \begin{bmatrix} X_1 & Y_1 & 0 & \cdots & \cdots & 0 & Z_1 \\ Z_2 & X_2 & Y_2 & 0 & \cdots & \cdots & 0 \\ 0 & Z_3 & X_3 & Y_3 & 0 & \cdots & 0 \\ \vdots & \vdots & \vdots & \vdots & \vdots & \vdots & \vdots \\ Y_{24} & 0 & \cdots & \cdots & 0 & Z_{24} & X_{24} \end{bmatrix} \quad (13)$$

Now define the following MMF's for the first 23 loops

$$F_n = F_{tooth(n+1)} + F_{PM(n+1)} - F_{PM(n)} - F_{tooth(n)} \quad (14)$$

and the loop 24 MMF is

$$F_{24} = F_{tooth1} + F_{PM1} - F_{PM24} - F_{tooth24} \quad (15)$$

We now define the following two vectors

$$\phi \equiv \begin{bmatrix} \phi_1 \\ \phi_2 \\ \vdots \\ \phi_{24} \end{bmatrix} \quad (16)$$

$$\mathbf{F} \equiv \begin{bmatrix} F_1 \\ F_2 \\ \vdots \\ F_{24} \end{bmatrix} \quad (17)$$

Using Eq. (3) through (17), our model is described as

$$\Re \phi = \mathbf{F} \quad (18)$$

and by rearranging Eq. (18), solution for flux is thus

$$\phi = \Re^{-1} \mathbf{F} \quad (19)$$

Because reluctances and MMF source values are dependant on flux density, this model is solved iteratively. First, an initial value of flux is assumed, and flux densities are calculated. Using the B-H curve for the metal parts (Figure 7) and knowledge of the mechanical gap size, reluctances for the metal parts and the air gap are calculated. The demagnetization curve (Figure 8) is used to generate the PM MMF at this flux density level, and the user-selected phase currents are used to calculate the tooth MMF. Equation 19 is then solved using the calculated source and reluctance values, providing new values of loop fluxes, and the process is repeated until the flux converges to a satisfactory limit.

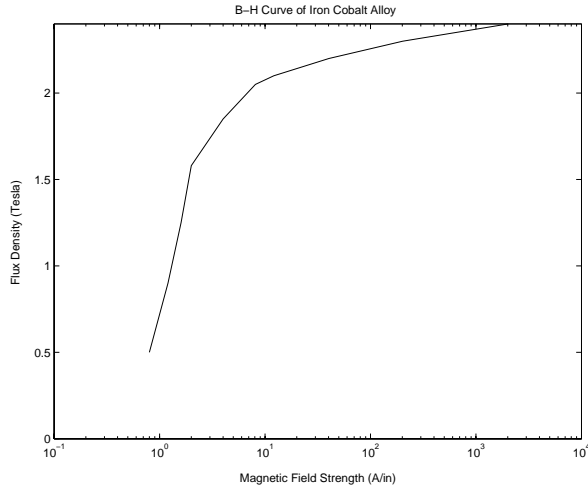


Figure 7. B-H curve of selected iron-cobalt alloy

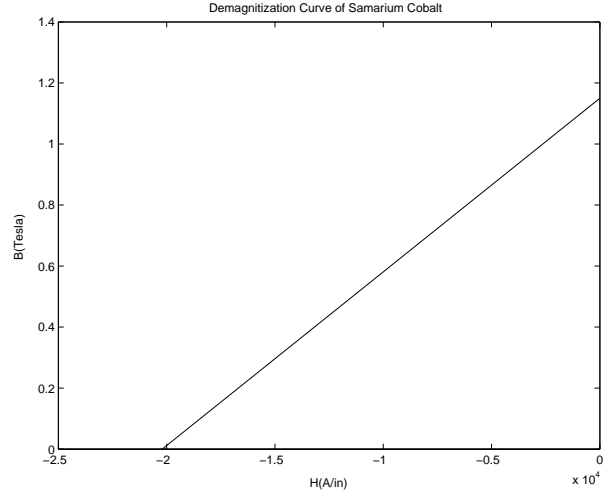


Figure 8. Demagnetization curve of PM material

Simulation Results

The motor simulation approach described in the previous section was used to calculate flux linkages and back EMF, motor torque and power, and rotor force. Details of these simulations are presented in the following sections.

Flux Linkage and Back EMF

The flux linkages are calculated by first running the simulation described in the previous section. Flux linking every individual coil is calculated, and individual coil fluxes in a phase belt are added together to obtain the flux linkages for each phase. A plot showing flux linkages for each phase is shown in Figure 9.

By performing time derivatives of the flux linkages, back EMF for each phase is then calculated using Faraday's law of induction:

$$v_{emf} = -\frac{d\lambda}{dt} \quad (20)$$

The simulation results for the motor operating at the maximum flywheel speed of 60kRPM, displaying the back EMF for each phase, are shown in Figure 10. Note that, as desired, the third harmonic has been virtually eliminated.

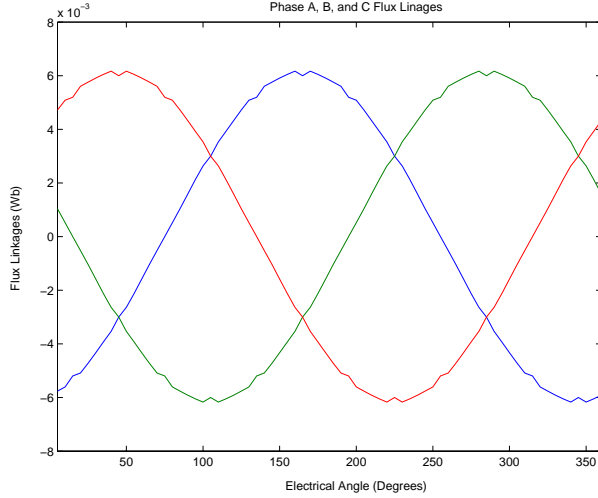


Figure 9. Flux linkages for phase A, B, and C

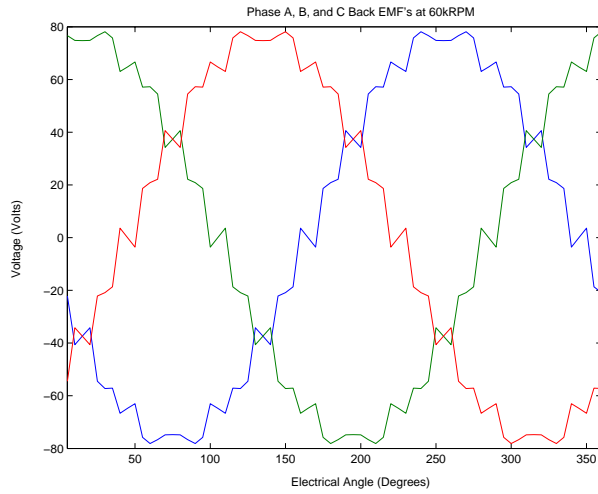


Figure 10. Back EMF's for phase A, B, and C

Motor Power and Torque

The instantaneous power delivered to the back EMF can be expressed as follows:

$$p = i_a v_{a-emf} + i_b v_{b-emf} + i_c v_{c-emf} \quad (21)$$

This power is equivalent to the mechanical power delivered to the rotor.

$$p = p_{mech} = \omega_{mech} \tau \quad (22)$$

where ω_{mech} is the mechanical angular velocity of the rotor and τ is the torque applied to the rotor. Combination of Eq. (21) and (22) yield the following expression for torque

$$\tau = \frac{i_a v_{a-emf} + i_b v_{b-emf} + i_c v_{c-emf}}{\omega_{mech}} \quad (23)$$

In order to calculate torque as a function of electrical angle, the simulation was run under constant phase current, with phase A current set to 1.0A (which automatically sets phase B and C currents at $-0.5A$). Individual simulations were run over an entire electrical revolution at five degree increments, using an arbitrarily selected zero degree point. The resultant torque plot is shown in Figure 11. Note that the maximum torque/amp generated by the motor is ~ 0.018 Nm/amp, and that this maximum will be achieved when the motor controller is aligned at about 255 electrical degrees. The ripples in the torque plot are due to back EMF perturbations, which are caused by the stator teeth.

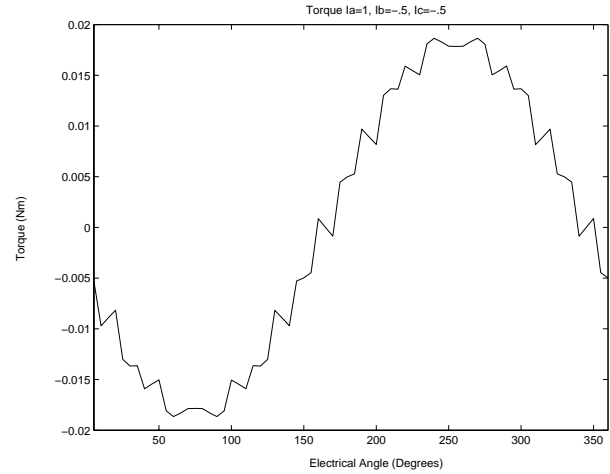


Figure 11. Generated torque versus electrical angle

Next, we wish to calculate motor power. Given the selected slot size and the current density of copper, and assuming the slot is filled with copper at a packing factor of 0.5, the maximum phase current the motor can draw is 122 A. Based on this, the previous simulation was run once again with constant phase A current of 122A (phase B and C at $-61A$). The result of this simulation, motor power as a function of electrical angle, is presented in Figure 12. Note that the maximum motor power under these conditions is $\sim 18KW$.

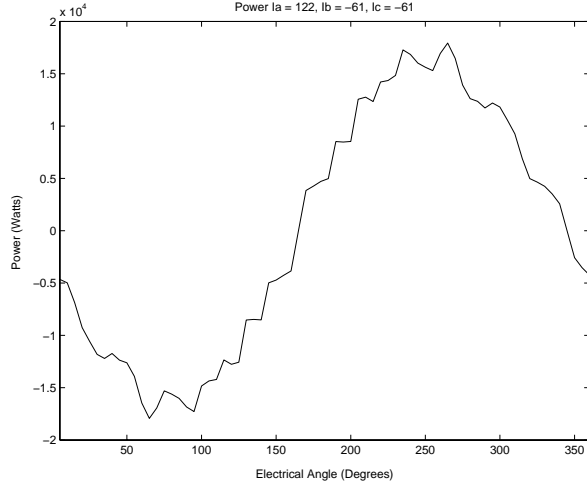


Figure 12. Maximum power versus electrical angle

Rotor Force Calculation

The forces the stator produces on the rotor are equal and opposite to the forces on the stator tooth tips. The magnitude of the forces on the tooth tips is given by [2]:

$$|F_{tooth-tip}| = \frac{A_{tooth-tip} \cdot B_{tooth-tip}^2}{2 \cdot \mu_0} \quad (24)$$

Since there are 24 teeth in the rotor, the rotor mechanical angle for each of the tooth locations can be expressed as

$$\theta_n = \frac{(n-1) \cdot 2 \cdot \pi}{24} \quad (25)$$

where $n = 1, 2, \dots, 24$. The general vector expression for force on the rotor at any of the tooth tips, from Eq. (24), is

$$F_n = \frac{A_{tooth-tip} \cdot B_{tooth-tip}^2}{2 \cdot \mu_0} [i \cdot \sin(\theta_n) + j \cdot \cos(\theta_n)] \quad (26)$$

Force on the rotor caused only by the PMs is calculated next, for the case of a rotor which is slightly displaced from center. This simulation is run with zero phase currents, with the rotor displaced in the +x direction, for an entire electrical revolution, using Eq. (26). Note that although the air gap for the motor is 200 mils total, the actual rotor motion is limited to ± 10 mils by the magnetic bearing system; thus, the displacement for this simulation was set to 10 mils. The result is presented in Figure 13. The x component of force has an average value of 13.45 lbs, with harmonics at 12 times the

electrical speed, which corresponds to harmonics that are at 24 times the mechanical spin speed (as expected with 24 teeth). Note also that the y component of force is zero; this means that all of the force on the rotor is in the radial direction.

Next, the previous simulation was run seven more times, each with a ten mil rotor displacement from center, at 45, 90, 135...315 mechanical degree locations around the rotor radial center point. With each simulation, force vectors on the rotor were calculated for an entire revolution. Each of these points, along with the data from Figure 13, are plotted in Figure 14. Note that the ripple caused by the teeth is present in each of these data sets, which explains why each of the data sets appears as a line. Note also that the force on the rotor in each of these simulations is in the radial direction.

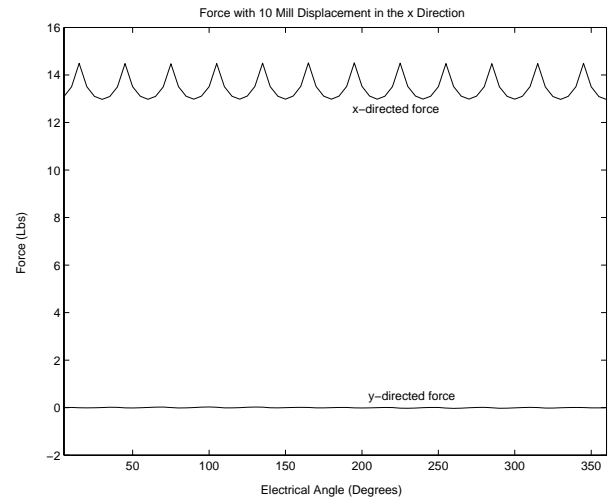


Figure 13: Force versus angle with 10 mil x-direction displacement

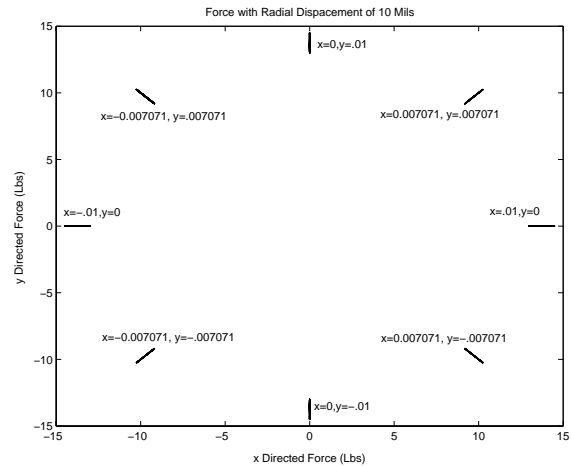


Figure 14. x and y force components with radial offsets of 10 mils, at 8 locations

Next, force versus position plots were generated, for small and large displacement values. Once again, the simulation was run with no phase current; separate simulations were run as the rotor was moved in the +x direction. Figure 15 shows the force versus displacement plot for small displacements (less than 2 mils) off center, and each plotted value is the average value of force over a 360 electrical degree rotation. This plot shows that the negative stiffness of the motor with the rotor close to the center is about 700 lbs/in. Note that for small displacements the negative stiffness is linear. Figure 16 shows force versus displacement for large displacements.

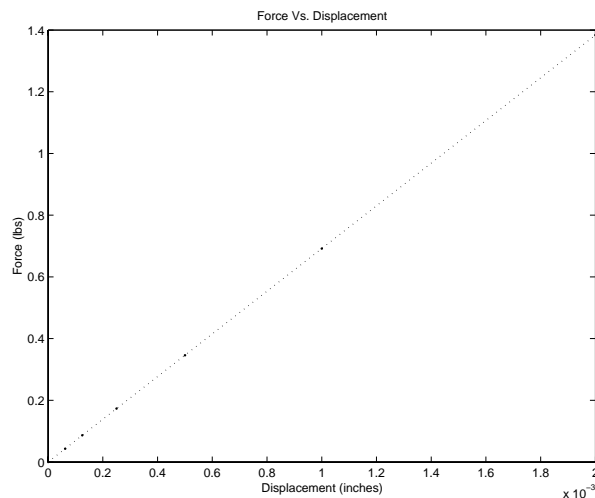


Figure 15. Force versus small displacement

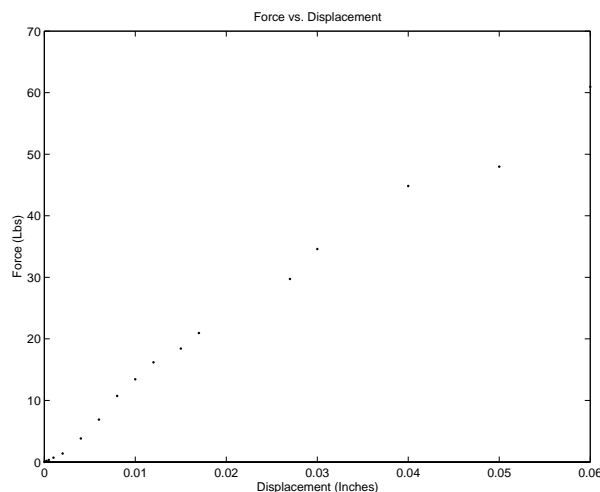


Figure 16. Force versus large displacement

Motor Design Summary

A summary of the motor design described in this paper is provided in Table 1.

Table 1. Motor design summary
(dimensions in inches)

Parameter	Design value
Poles	4
Turns/coil	1
Number of slots	24
Inner rotor diameter	1.0
Outer rotor diameter	2.75
Outer stator diameter	6.50
Magnet thickness	0.15
Mechanical air gap	0.20
Slot depth	0.394
Axial stack length	1.50
Yoke thickness	0.725
Back iron thickness	1.281
Slot pitch	0.4123
Tooth width at air gap	0.2062
Maximum speed	60kRPM
Motor power (kW @60kRPM)	18

Conclusions

This paper describes a detailed motor-generator circuit model and simulation approach. A sample design and simulation are presented, and the simulation predicts motor back EMF, power, and torque versus electrical angle for the specified design. Additionally, force due to the permanent magnets (zero motor currents) is calculated versus rotor displacement, yielding negative stiffness relationships; for small displacements of the rotor (<2 mils), the negative stiffness was found to be linear. Also, simulations at 10 mil displacements all around the rotor center revealed that only radial forces were exerted on the rotor by the permanent magnets.

References

1. Lipo, T.A., *Introduction to AC Machine Design*, University of Wisconsin, Madison, Wisconsin, 1996.
2. Schweitzer, G., Blueier, H. and Traxler, A., *Active Magnetic Bearings*, vdf Hochschulverlag AG and ETH, Zurich, 1994.

REPORT DOCUMENTATION PAGE			Form Approved OMB No. 0704-0188	
Public reporting burden for this collection of information is estimated to average 1 hour per response, including the time for reviewing instructions, searching existing data sources, gathering and maintaining the data needed, and completing and reviewing the collection of information. Send comments regarding this burden estimate or any other aspect of this collection of information, including suggestions for reducing this burden, to Washington Headquarters Services, Directorate for Information Operations and Reports, 1215 Jefferson Davis Highway, Suite 1204, Arlington, VA 22202-4302, and to the Office of Management and Budget, Paperwork Reduction Project (0704-0188), Washington, DC 20503.				
1. AGENCY USE ONLY (Leave blank)		2. REPORT DATE February 2004		3. REPORT TYPE AND DATES COVERED Final Contractor Report
4. TITLE AND SUBTITLE Magnetic Circuit Model of PM Motor-Generator to Predict Radial Forces			5. FUNDING NUMBERS WBS-22-755-60-15 NCC3-924	
6. AUTHOR(S) Peter E. Kascak, Timothy P. Dever, and Ralph H. Jansen				
7. PERFORMING ORGANIZATION NAME(S) AND ADDRESS(ES) University of Toledo 2801 W. Bancroft Street Toledo, Ohio 43606			8. PERFORMING ORGANIZATION REPORT NUMBER E-14178	
9. SPONSORING/MONITORING AGENCY NAME(S) AND ADDRESS(ES) National Aeronautics and Space Administration Washington, DC 20546-0001			10. SPONSORING/MONITORING AGENCY REPORT NUMBER NASA CR-2004-212620 AIAA-2003-6068	
11. SUPPLEMENTARY NOTES Prepared for the First International Energy Conversion Engineering Conference sponsored by the American Institute of Aeronautics and Astronautics, Portsmouth, Virginia, August 17-21, 2003. Peter E. Kascak and Ralph H. Jansen, University of Toledo, Toledo, Ohio 43606; and Timothy P. Dever, QSS Group, Inc., Cleveland, Ohio 44135. Project Manager, Kerry McLallin, Power and Propulsion Office, NASA Glenn Research Center, organization code 6910, 216-433-5389.				
12a. DISTRIBUTION/AVAILABILITY STATEMENT Unclassified - Unlimited SubjectCategories: 20, 33, 37, 44, and 88 Distribution: Nonstandard Available electronically at http://gltrs.grc.nasa.gov This publication is available from the NASA Center for AeroSpace Information, 301-621-0390.			12b. DISTRIBUTION CODE	
13. ABSTRACT (Maximum 200 words) A magnetic circuit model is developed for a PM motor for flywheel applications. A sample motor is designed and modeled. Motor configuration and selection of materials is discussed, and the choice of winding configuration is described. A magnetic circuit model is described, which includes the stator back iron, rotor yoke, permanent magnets, air gaps and the stator teeth. Iterative solution of this model yields flux linkages, back EMF, torque, power, and radial force at the rotor caused by eccentricity. Calculated radial forces are then used to determine motor negative stiffness.				
14. SUBJECT TERMS Motor; Generator; Magnetic circuit; Model; Flywheel			15. NUMBER OF PAGES 14	
			16. PRICE CODE	
17. SECURITY CLASSIFICATION OF REPORT Unclassified	18. SECURITY CLASSIFICATION OF THIS PAGE Unclassified	19. SECURITY CLASSIFICATION OF ABSTRACT Unclassified	20. LIMITATION OF ABSTRACT	